Magnetic structure determination of Ca₃LiOsO₆ using neutron and x-ray scattering

S. Calder,[1,*] M. D. Lumsden,[1] V. O. Garlea,[1] J. W. Kim,[2] Y. G. Shi,[3,4] H. L. Feng,[4,5] K. Yamaura,[4,5] and A. D. Christianson[1]

[1]*Quantum Condensed Matter Division, Oak Ridge National Laboratory, Oak Ridge, Tennessee 37831, USA*
[2]*Advanced Photon Source, Argonne National Laboratory, Argonne, Illinois 60439, USA*
[3]*Institute of Physics, Chinese Academy of Sciences, 100190 Beijing, China*
[4]*Superconducting Properties Unit, National Institute for Materials Science, 1-1 Namiki, Tsukuba, Ibaraki 305-0044, Japan*
[5]*Graduate School of Chemical Sciences and Engineering, Hokkaido University, Sapporo, Hokkaido 060-0810, Japan*

We present a neutron and x-ray scattering investigation of Ca₃LiOsO₆, a *5d* material predicted to host magnetic ordering solely through an extended superexchange pathway involving two anions. This contrasts with investigations of extended superexchange interactions that have been largely limited to low-dimensional *3d* systems involving both superexchange and extended superexchange. Despite the apparent one-dimensional nature and triangular units of magnetic osmium ions in Ca₃LiOsO₆, the onset of magnetic correlations has been observed at a high temperature of 117 K in bulk measurements. We experimentally determine the magnetically ordered structure and show it to be long range and three dimensional. Our results support the model of extended superexchange interaction.

PACS number(s): 75.10.Lp, 75.25.−j, 75.70.Tj, 71.30.+h

I. INTRODUCTION

The investigation of *5d* transition-metal oxides (TMO) has resulted in the observation of a variety of novel properties due to the competition of spin-orbit coupling (SOC), onsite Coulomb interaction, and crystal-field splitting that are all of comparable strength. This contrasts with the much more studied *3d* TMO in which spin-orbit coupling is generally only a small perturbation. On the other hand, the radius of the electronic wave function is extended in *5d* systems compared to *3d* TMO, resulting in increased itinerant properties. Much of the recent experimental and theoretical focus on *5d* TMO has concentrated on iridates due to the observance of a so-called $J_{\text{eff}} = 1/2$ Mott spin-orbit insulating state. This state arises due to the SOC splitting of the t_{2g} manifold as a consequence of the $5d^5$ electron configuration. Consequently, even small onsite Coulomb interactions can result in insulating behavior.[1] Iridates have been found to host topological insulating states,[2] Weyl semimetal,[3] and potentially the Kitaev model.[4]

Systems containing the neighboring osmium ion have also showed interesting properties. For example, NaOsO₃ undergoes a Slater metal-insulator transition[5] and KOs₂O₆ is an unconventional superconductor.[6] We focus on an additional compound of note, Ca₃LiOsO₆, that was grown and characterized by Shi *et al*.[7] Ca₃LiOsO₆, an insulator at at all temperatures we consider, forms the K₄CdCl₆-type crystal structure (hexagonal space group $R\bar{3}c$) in which apparent one-dimensional (1D) chains of Os ions along the *c* axis are separated by Li ions in a frustrated geometry, as shown in Fig. 1. However, the high magnetic ordering temperature reported of 117 K is not compatible with this quasi-1D frustrated picture.[7] Instead, the authors presented a model for Ca₃LiOsO₆ containing extended superexchange magnetic interactions of Os-O-O-Os to account for the high magnetic ordering temperature. Shortly after, a theoretical investigation supported this model and considered possible magnetic exchange interactions.[8] While magnetic interactions mediated by a single anion are common with long-standing and well-defined Goodenough-Kanamori rules,[9] the investigation of materials with solely the extended

superexchange interaction through two anions has undergone relatively little investigation.

We have performed a neutron and magnetic x-ray scattering investigation to determine the magnetic structure of Ca₃LiOsO₆. The related *4d* material Ca₃LiRuO₆ also undergoes a magnetic transition at a similar temperature, suggestive that the electronic configuration of d^3 is significant and plays a role in the magnetic ordering.[10] For Ca₃LiOsO₆, we find a magnetic structure in which both interchain and intrachain magnetic interactions are present. The magnetic model is three dimensional (3D) and contains no geometric frustration, making it compatible with the high magnetic ordering temperature observed and the low ratio of Θ_W/T_N from susceptibility.[7] We present both powder and single-crystal results that confirm the magnetic ordering temperature and are consistent with a magnetic structure that involves solely the extended superexchange interaction. Ca₃LiOsO₆, along with Ca₃LiRuO₆, appear to be ideal candidates to investigate the extended superexchange interaction. Unlike the iridates discussed above in which the $5d^5$ electronic configuration leads to the degeneracy of the t_{2g} level being broken by spin-orbit coupling, the $5d^3$ configuration is expected to remain degenerate, even for the case of large SOC.[11] We consider the t_{2g} configuration through an interpretation of our neutron and x-ray results.

II. EXPERIMENTAL METHODS

Single-crystal and polycrystalline samples of Ca₃LiOsO₆ were prepared as described in Ref. 7. Neutron powder diffraction (NPD) measurements were performed at the High Flux Isotope Reactor (HFIR) at Oak Ridge National Laboratory (ORNL) using beamline HB-2A. Measurements were performed with both $\lambda = 1.54$ Å and $\lambda = 2.41$ Å on a 5 g sample. The shorter wavelength gives a greater intensity and higher Q coverage that we utilized to investigate the crystal structure through the magnetic phase transition from 150 to 30 K. The longer wavelength gives lower $|Q|$ coverage and
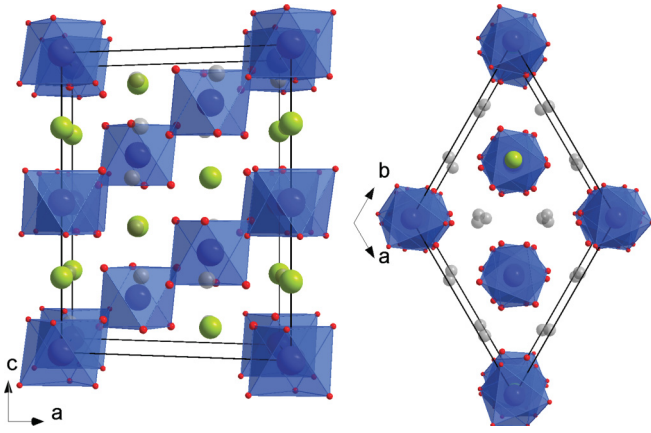
FIG. 1. (Color online) Ca_3LiOsO_6 forms a hexagonal crystal structure with space group $R\bar{3}c$. Magnetic Os^{5+} ions (blue spheres) are surrounded by six oxygen anions (red spheres). These octahedra are separated along the c axis by Li^+ ions. Ca^{2+} ions (gray spheres) provide the charge balance.

greater resolution that we employed to investigate the magnetic structure at 4 K, with a comparable measurement at 150 K. The NPD data were investigated using the Rietveld refinement program FULLPROF (see Table I) and the magnetic structural representational analysis was performed using SARA*h*.[12]

The triple-axis instrument HB1 at HFIR was used in elastic mode with a wavelength of 2.46 Å to investigate the magnetic order parameter at the (101) magnetic reflection on the same powder sample. Various measurements were taken from 10 K through the magnetic transition temperature of ~117 K. The integrated intensity of the scattering around the magnetic

reflection was calculated to determine the magnetic ordering temperature.

A single-crystal investigation on a crystal of approximate size $0.1 \times 0.1 \times 0.05$ mm was performed at the Advanced Photon Source (APS) at beamline 6-ID-B using magnetic resonant x-ray scattering (MRXS). We carried out measurements at both the $L2$ and $L3$ resonant edges of osmium that correspond to 12.393 and 10.878 keV, respectively. Graphite was used as the polarization analyzer crystal at the (0 0 10) and (008) reflections on the $L2$ and $L3$ edges, respectively, to achieve a scattering angle close to $90°$. For the $L3$ edge, the scattering angle was $86°$ and for $L2$ the scattering angle was $94°$. Measurements were taken at several reflections to investigate possible magnetic structures, with an analysis of the photon polarization in σ-σ and σ-π allowing a distinction between magnetic and charge scattering. To account for absorption, energy scans were performed without the analyzer and with the detector away from any Bragg peaks through both absorption energies.

III. RESULTS AND DISCUSSION

A. Neutron diffraction crystal-structure investigation

We investigated the crystal-structure temperature variation of Ca_3LiOsO_6 using NPD from 150 to 4 K, through the magnetic anomaly observed around 117 K.[7] Our NPD results at 4 and 150 K are consistent with previously reported x-ray diffraction (XRD),[7] which showed no structural symmetry change (see Fig. 2). The results are not conclusive to assign the possibility of a structurally driven magnetic transition and any anomaly is much less pronounced than from XRD.[7]

TABLE I. Refined crystal-structure parameters from FULLPROF for (a) 150 K and (b) 4 K for $\lambda = 1.54$ Å.

(a) 150 K

		Space group	$R\bar{3}c$		
		a	9.257(1) Å		
		c	10.763(1) Å		
		Cell volume	798.86(1) Å^3		
		χ^2	4.30		
		R_{wp}	5.99%		

Atom	site	x	y	z	B_{iso} (Å^2)
Os	6b	0	0	0	0.366(4)
Ca	18e	0.6460(3)	0	0.25	0.333(5)
O	36f	0.0281(14)	0.8438(1)	0.3942(2)	0.610(3)
Li	6a	0	0	0.25	1.54(2)

(b) 4 K

		Space group	$R\bar{3}c$		
		a	9.249(1) Å		
		c	10.758(1) Å		
		Cell volume	797.02(1) Å^3		
		χ^2	5.85		
		R_{wp}	5.83%		

Atom	site	x	y	z	B_{iso} (Å^2)
Os	6b	0	0	0	0.293(3)
Ca	18e	0.6458(3)	0	0.25	0.209(4)
O	36f	0.0279(2)	0.8437(2)	0.3940(2)	0.483(3)
Li	6a	0	0	0.25	1.14(2)

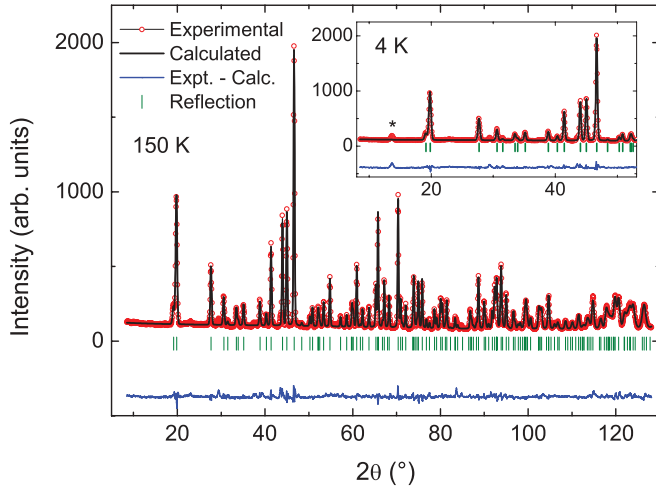FIG. 2. (Color online) Neutron powder diffraction results at 150 and (inset) 4 K with $\lambda = 1.54$ Å measured on HB-2A at HFIR. The crystal-structure symmetry remains unchanged between high and low temperature, however, an additional magnetic reflection indicative of magnetic order is observed at low temperature, indicated by the asterisk.

B. Magnetic structure

1. Neutron powder diffraction

The crystal structure of Ca_3LiOsO_6 has each osmium ion surrounded by six oxygen ions in an octahedral environment (see Fig. 1). The octahedra remain invariant with a- or b-axis translations, but their orientation alternate along the c axis. In a model of extended magnetic superexchange interaction, the octahedra form the Os-O-O-Os exchange pathway. The temperature variation of the Os-O distance obtained from NPD shows virtually no deviation with temperature. The electronic configuration of the Os^{5+} ion is $5d^3$, with the three electrons therefore expected to each occupy the crystal-field-split degenerate t_{2g} orbitals d_{xy}, d_{yz}, and d_{zx}. Reference 7 discusses the possibility of a trigonal crystalline electric field (CEF) breaking of the t_{2g} degeneracy. If this degeneracy were broken, it would be expected that this would be reflected in a deviation of the Os-O bonds within the octahedra, however, this is not observed. Similarly, any Jahn-Teller distortions are precluded by the lack of variation in the Os-O distance. Therefore, our results show no indication that the t_{2g} degeneracy that results due to the crystal-field splitting of octahedrally coordinated oxygens anions around the magnetic ion being further split by spin-orbit interactions, as occurs in certain iridates.

B. Magnetic structure

1. Neutron powder diffraction

The NPD measurements showed additional scattering at commensurate positions below $\sim$120 K indicative of magnetic ordering. To determine the nature of the magnetic order, we implemented representational analysis.[12] For a second-order transition, Landau theory states that the symmetry properties of the magnetic structure are described by only one irreducible representation (IR). All the magnetic reflections can be indexed using a propagation vector $\mathbf{k} = (000)$, therefore, this was employed in our analysis. For the $R\bar{3}c$ crystal structure with the magnetic moment on the Os ion and commensurate propagation vector $\mathbf{k} = (000)$, there are three possible IRs.

TABLE II. Basis vectors (BV) for the space group $R\text{-}3c : H$ with $\mathbf{k} = (0,0,0)$. The decomposition of the magnetic representation for the Os site $(0,0,0)$ is $\Gamma_{Mag} = 1\Gamma_1^1 + 0\Gamma_2^1 + 1\Gamma_3^1 + 0\Gamma_4^1 + 2\Gamma_5^2 + 0\Gamma_6^2$. The atoms of the nonprimitive basis are defined according to 1: $(0,0,0)$, 2: $(0,0,\frac{1}{2})$.

IR	BV	Atom	BV components					
			$m_{\|a}$	$m_{\|b}$	$m_{\|c}$	$im_{\|a}$	$im_{\|b}$	$im_{\|c}$
Γ_1	ψ_1	1	0	0	1	0	0	0
		2	0	0	-1	0	0	0
Γ_3	ψ_2	1	0	0	1	0	0	0
		2	0	0	1	0	0	0
Γ_5	ψ_3	1	6	0	0	0	0	0
		2	0	0	0	0	0	0
	ψ_4	1	0	0	0	0	0	0
		2	-1	-1	0	0	0	0
	ψ_5	1	0	0	0	0	0	0
		2	-1	1	0	0	0	0
	ψ_6	1	-1	-1	0	0	0	0
		2	0	0	0	0	0	0

Table II lists the IR and corresponding basis vectors ψ. The IR correspond to $\Gamma(1)$, $\Gamma(3)$, and $\Gamma(5)$ (following the numbering scheme of Kovalev[13]). $\Gamma(3)$ could be readily discarded as not giving scattering at the correct reflections for the magnetic ordering. Figure 3 shows the refined model for the $\Gamma(1)$ and $\Gamma(5)$ IRs. Refining both models to fit the experimental scattering does not produce conclusively different results to allow for the definition of a unique magnetic structure, despite relatively large counting times performed during the NPD.

Although the scattering is well reproduced by both models, there is a clear distinction between the magnetic structure they represent. The two candidate magnetic structures are shown schematically in Figs. 3(c) and 3(d). $\Gamma(1)$ has spins Antiferromagnetically (AFM) aligned along the c axis in 1D chains, for which 3D ordering would be frustrated due to the triangular units between the chains. $\Gamma(5)$ has spins oriented in the a-b plane that would require extended superexchange Os-O-O-Os interactions to describe the 3D ordering.

There are certain distinctions between the modeled neutron scattering for each IR. First, for $\Gamma(1)$ there is no scattering at the reflection at $\sim$40° that corresponds to (003), while there is scattering for the $\Gamma(5)$ model. Second, the scattering at the magnetic peaks is slightly better modeled for the $\Gamma(5)$ model compared to the $\Gamma(1)$ model as evidenced by the χ^2 value being slightly lower for the $\Gamma(5)$ model. As shown in Table II, there is only one basis vector (BV), ψ_1, for $\Gamma(1)$. Therefore, there are only moments allowed oriented in the c axis and consequently the only variable is the size of the magnetic moment. The refinement for this $\Gamma(1)$ model gives a magnetic moment of $\sim$2μ_B. Conversely, for $\Gamma(5)$ there are four basis vectors, which all only allow moments in the a-b plane. In the basal plane, any angle between spins is possible. However, placing the spins at an angle of 90° or less results in an intensity mismatch on the lowest two observed angular reflections and can be readily discarded as a valid model. In the IR analysis, the atoms of the nonprimitive basis are defined according to 1: $(0,0,0)$, 2: $(0,0,\frac{1}{2})$. These two sites sit at equivalent atomic environments and so we consider
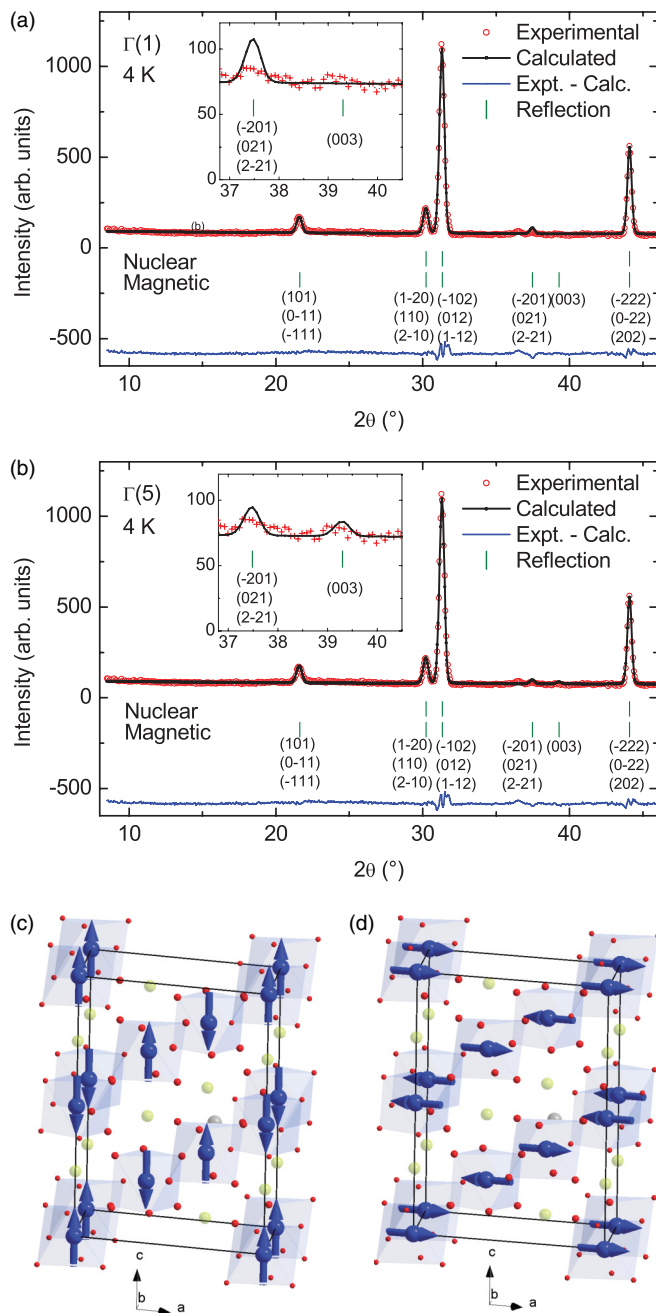
FIG. 3. (Color online) NPD data with $\lambda = 2.41$ Å at 4 K modeled with two possible magnetic structures from the representational analysis, labeled (a) $\Gamma(1)$ and (b) $\Gamma(5)$, following the numbering scheme of Kovalev. The refinement gave (a) R_p 5.10, $R_{wp} = 7.21$, $R_{exp} = 2.82$, $\chi^2 = 6.54$ and (b) $R_p = 4.98$, $R_{wp} = 7.02$, $R_{exp} = 2.83$, $\chi^2 = 6.17$. The corresponding magnetic spin structure is shown for (c) $\Gamma(1)$ and (d) $\Gamma(5)$. The schematic shows 180° between spins, however, additional angles are possible in the basal plane as described in the text.

the constraint that the magnitude of the spins on both sites should be the same and the orientation restricted to equivalent directions in the hexagonal crystal structure. Using different basis-vector values with these constraints produces magnetic models with fixed angles of 120° and 180° between the spins in the basal plane as physically reasonable models. The modeled

intensity is different for different values of BVs at the allowed reflections for $\Gamma(5)$. However, the sharp fall of the form-factor dependence for Os^{5+} results in appreciably no discernible difference between the various BV values with angles between spins of 120° and 180°. Consequently, from the NPD data for the $\Gamma(5)$ model, we are able to define the the magnetic moment as falling in the range $2.0\mu_B$ to $2.3\mu_B$, with the spins in the *a-b* plane.

Both $\Gamma(1)$ and $\Gamma(5)$ models give a reduced magnetic moment from the spin-only $S = 3/2$ value of $3\mu_B$ of between 66% to 76%. This is reduced from that predicted by a Curie-Weiss fit to the susceptibility that produced 98% of the expected spin-only model.[7] A reduced moment from that expected by a localized spin model, and even that found from a Curie-Weiss fit, has been observed for various $5d$ TMO systems.[14] The extended radius of $5d$ systems would be expected to result in a greater tendency away from a purely localized spin model and consequently a larger degree of covalency and charge fluctuations has been postulated to describe this behavior.[15]

2. Magnetic resonant x-ray scattering

To distinguish between the $\Gamma(1)$ and $\Gamma(5)$ magnetic models, we extended our investigation to a single crystal of Ca_3LiOsO_6 using magnetic resonant x-ray scattering (MRXS) at the APS. MRXS has several unique qualities, specifically for our investigation is the ability to measure magnetic scattering using small single crystals of dimensions inaccessible to neutron scattering. Additionally, MRXS directly probes electronic excitations within the magnetic ion and therefore allows a consideration of the role of the increased SOC in $5d$ systems, as has been previously shown using MRXS.[1] In general, $5d$ systems are particularly well suited to MRXS and show large resonant enhancements at certain well-defined energies.[1,16,17] For osmium, these resonant edges are labeled $L2$ and $L3$ and correspond to energies of 12.393 and 10.878 keV, respectively, for Ca_3LiOsO_6. The $L3$ absorption corresponds to electronic $2p_{\frac{3}{2}} \rightarrow 5d$ transitions and the $L3$ edge corresponds to $2p_{\frac{1}{2}} \rightarrow 5d$ electronic transitions. The crystal environment plays a role in determining the exact resonant energies observed away from that of an isolated single ion, however, we note that Ca_3LiOsO_6 and the recently measured $NaOsO_3$ produced virtually the same resonant energy values and energy peak shapes.[5] This suggests a similar local environment and electronic configuration for the Os^{5+} ion in both systems. We observed a strong magnetic resonant enhancement at both $L2$ and $L3$ edges for Ca_3LiOsO_6. This is compatible with a lack of splitting of the t_{2g} degeneracy by spin-orbit coupling, as was observed for $NaOsO_3$. These results contrast with iridates with a $J_{eff} = 1/2$ insulating state in which there is virtually no resonant enhancement at the $L2$ edge.[1]

We performed a thorough analysis of various magnetic and nonmagnetic reflections using MRXS to distinguish between the two candidate magnetic structures from NPD. To determine if the observed scattering was magnetic or nonmagnetic (or both), we performed a polarization analysis of the scattered x-ray beam. This exploits the fact that an incident x-ray beam of linearly polarized light is rotated by 90° when scattered by magnetic dipoles. Therefore, for σ-σ polarization there is no
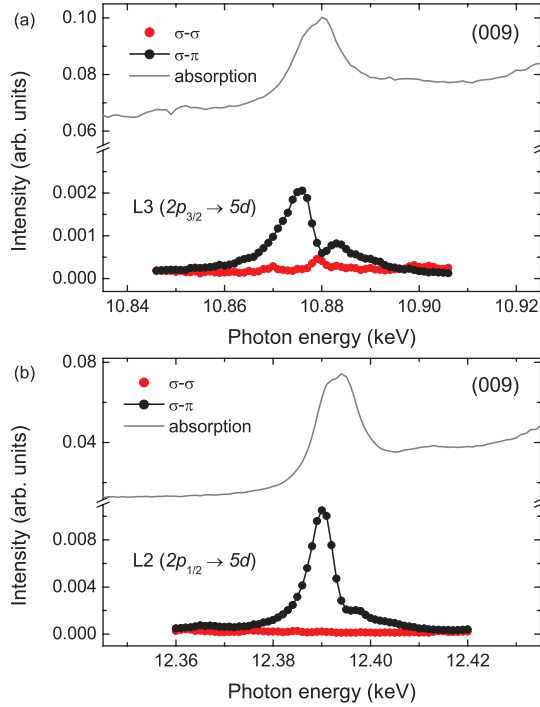
FIG. 4. (Color online) MRXS energy dependence of the (009) reflection. There is a large enhancement observed in the σ-π scattering and a suppression of scattering in the σ-σ channel, as expected for a purely magnetic reflection. A large resonant enhancement was observed at both $L2$ and $L3$ edges.

TABLE III. Measured reflections of Ca_3LiOsO_6 using MRXS. Those marked (*) are reflections corresponding to only the $\Gamma(5)$ model.

Reflection	Magnetic
(0 0 3)*	Yes
(1 −1 5)	Yes
(2 0 5)	Yes
(5 0 5)	Yes
(1 0 7)	Yes
(0 −1 7)	Yes
(−1 1 7)	Yes
(−1 −2 7)	Yes
(4 0 7)	Yes
(0 0 9)*	Yes
(−2 2 11)	Yes
(−1 0 11)	Yes
(0 1 11)	Yes
(1 −1 11)	Yes
(0 −2 11)	Yes
(0 0 15)*	Yes
(−1 0 7)	No scattering
(0 1 7)	No scattering
(1 1 9)	Magnetic and charge scattering
(1 2 11)	Magnetic and charge scattering

intensity if the scattering is magnetic, whereas σ-π polarization produces a large enhancement around the resonant edges for magnetic scattering. This is demonstrated in Fig. 4 for the (009) purely magnetic reflection. We performed measurements above and below the magnetic transition temperature to rule out the possibility of the (009) intensity being due to Templeton (ATS) scattering. To confirm the consistency of our distinction between magnetic and nonmagnetic reflections, we measured all permutations of a select reflection: (107), (0-17), (−117), (−107), and (017) and found the correct nature of scattering for the crystal and magnetic structures. We measured the reflections at the same azimuth to limit the possibility that the zero intensities were azimuth or moment direction dependent.

Table III lists the measured peaks of Ca_3LiOsO_6 in our investigation and the nature of the scattering. All the magnetic reflections are consistent with that of the $\Gamma(5)$ model, with those marked with an asterisk not allowed for the $\Gamma(1)$ model. Therefore, taking all our neutron and x-ray results support the $\Gamma(5)$ model, with spins oriented in the a-b plane, as being the ordered magnetic structure for Ca_3LiOsO_6.

One question remains as to the specific direction of each spin in the a-b plane or if indeed there is a specific direction or a random arrangement due to domains. Since rotating the spins equally around the a-b plane results in appreciably the same modeled scattering from neutron diffraction, this could not be used to distinguish between directions. Additionally, we performed azimuthal scans that can give definitive information

on the moment direction, however, we observed no obvious trends. Regardless of the specific spin direction, the relative arrangement of each spin with respect to their neighbor and next-nearest neighbor remains the same and therefore our discussion of the exchange interactions in Sec. III B4 does not depend on the definition of a unique spin direction.

3. Magnetic ordering temperature of Ca3LiOsO6

Having experimentally determined the magnetic structure for Ca_3LiOsO_6, we now consider the antiferromagnetic ordering temperature T_N. We measured the scattering around the (101) reflection $|Q| = 0.97 \text{ Å}^{-1}$, with elastic neutron scattering on beamline HB1 at HFIR and the scattering around the (107), $|Q| = 4.16 \text{ Å}^{-1}$, reflection at the $L2$ edge with MRXS on beamline 6-ID-B at the APS. The integrated intensity for the various temperature measurements is shown in Fig. 5. We fit the temperature dependence of the integrated intensity to a power law to determine the magnetic ordering temperature and allow an estimate of the β exponent. From the neutron scattering results on a powder sample, we find $T_N = 117.1 \pm 0.9$ K. The associated exponent is $\beta = 0.28 \pm 0.1$; however, we stress that obtaining critical scattering from our data is not feasible and instead only note that the exponent is closer to the 3D value. We note that the observance of scattering along h, k, and l in a single crystal using MRXS is more direct evidence that the magnetic order is 3D. MRXS gives a AFM ordering temperature of $T_N \approx 115$ K, however, due to sample heating issues, the reliability in sample temperature results in unassignable error bars and as such we simply note that the value is consistent with neutron scattering and bulk data.[7] Additionally, we can not rule out that there may exist a
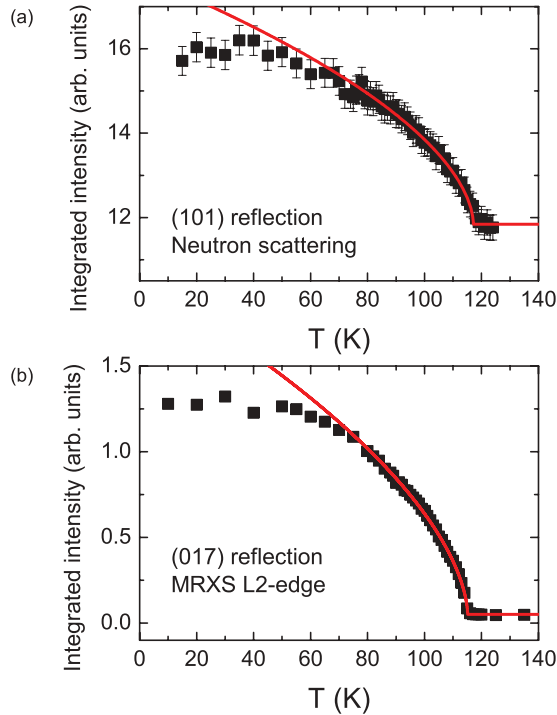
FIG. 5. (Color online) Integrated intensity of the scattering at purely magnetic reflections with (a) powder neutron scattering and (b) single-crystal MRXS. The determined antiferromagnetic transition ordering temperature T_N is shown to agree for both techniques.

FIG. 6. (Color online) Schematic of magnetic structure of Ca_3LiOsO_6. Blue spheres are Os ions with associated magnetic spin shown as an arrow. Smaller red spheres are oxygen ions. (a) Magnetic extended superexchange pathways Os-O-O-Os: J_1 (black), J_2 (red), and J_3 (blue). J_1 and J_2 form AFM exchange interactions, whereas J_3 forms FM bonds. (b)–(d) The separate magnetic interaction pathways are shown with their respective distances and angles. The angle between spins in the schematic is $180°$. See the text for discussion of other angles, however, we note that altering the angle between spins does not effect our discussion of the different exchange interactions.

difference between the powder and single-crystal samples that results in slightly different ordering temperatures. The order parameter from both techniques has all the hallmarks for 3D order, and does not show the sharp increase associated with 2D ordering. Therefore, within experimental error, the neutron and x-ray results agree and correspond to the transition temperature observed in susceptibly and specific-heat measurements in the literature.[7]

4. *Magnetic exchange interactions*

The magnetic spins reside on the *a-b* plane and form 3D magnetic order that is best explained as involving the extended superexchange magnetic interaction pathway Os-O-O-Os. The extended superexchange interactions are shown in Fig. 6, labeled J_1, J_2, and J_3. Kan *et al.* considered the relative strength of these exchange interactions using density functional theory calculations for Ca_3LiOsO_6 for various AFM or FM interactions.[8] Considering Fig. 6, the magnetic structure for Ca_3LiOsO_6 we have presented gives J_1 spins oppositely aligned, J_2 spins oppositely aligned, and J_3 spins coaligned. Kan *et al.* considered four possible magnetic structures and concluded that all J_1, J_2, and J_3 interactions were AFM, whereas the experimentally determined magnetic structure presented here has J_3 spins parallel. The overall Os-Os bond length increases in going from J_1 (5.38 Å) to J_2 (5.64 Å) to J_3 (6.43 Å). However, since the magnetic structure involves 3D interactions, the magnetic ordering can not simply be described in terms of the shortest J_1 interaction along the
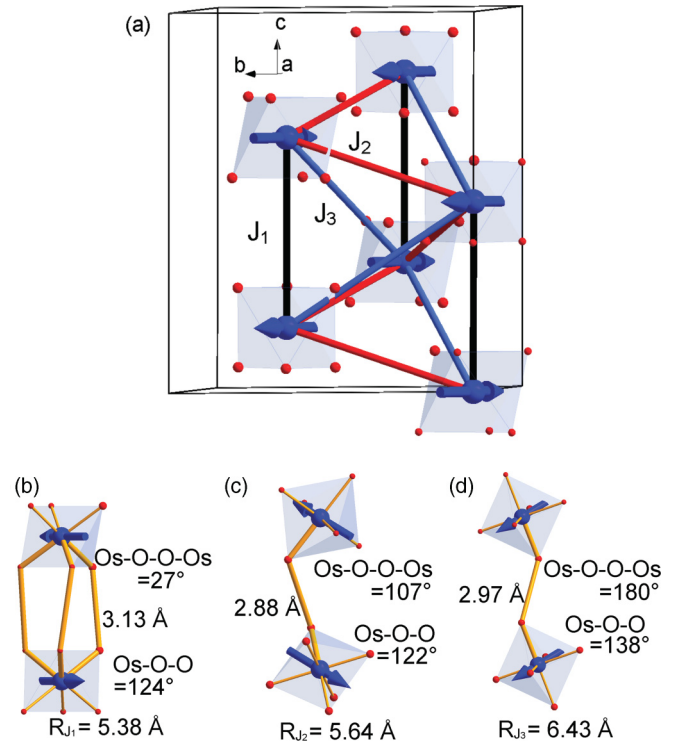
c axis. Therefore, the further exchange interactions J_2 and J_3 are required. Since frustration effects are negligible, this requires that J_2 and J_3 not be of a similar strength, as noted previously.[8] This would be compatible with J_1 and J_2 having large negative AFM values, while J_3 is small and consequently is fixed according to the J_1 and J_2 interactions and produces apparent FM interactions, even though the J_3 exchange interaction is negative. However, one alternative conclusion for J_3 spins being parallel could be argued in terms of the bond angles between the three different Os-O-O-Os pathways favoring FM interactions, considered in Figs. 6(b)–6(d). For J_1 and J_2 the Os-O-O bond angle is approximately equivalent to $90°$ and the torsion angle of Os-O-O-Os deviates from $90°$ by approximately the same value. Comparing J_1 and J_2 with J_3 shows markedly different Os-O-O and Os-O-O-Os bond angle values. Therefore, the oxygen *p* orbitals and Os t_{2g} *d* orbitals will overlap differently for J_3, compared to J_1 and J_2. It would be of interest to theoretically calculate stable J_1-AFM, J_2-AFM, and J_3-FM values compatible with the magnetic structure for Ca_3LiOsO_6 we have reported.

IV. CONCLUSION

We have presented a combined neutron and x-ray scattering investigation of Ca_3LiOsO_6. The results are compatible with a magnetic structure of $\Gamma(5)$ (following the numbering scheme of Kovalev) in which the spins are in the *a-b* plane. The magnetic order is 3D and can be explained in terms of a model of Os-O-O-Os extended superexchange interactions. Despite apparent triangular units, frustration is relieved as a consequence of the nature of the Os-O-O-Os pathways present that involve both AFM and FM exchange interactions. Ca_3LiOsO_6 provides an ideal model to investigate the magnetic extended superexchange interaction free from any single-anion superexchange effects.

---

*caldersa@ornl.gov

[1] B. J. Kim, H. Ohsumi, T. Komesu, S. Sakai, T. Morita, H. Takagi, and T. Arima, Science **323**, 1329 (2009).

[2] D. Pesin and L. Balents, Nat. Phys. **6**, 376 (2010).

[3] X. Wan, A. M. Turner, A. Vishwanath, and S. Y. Savrasov, Phys. Rev. B **83**, 205101 (2011).

[4] J. Chaloupka, G. Jackeli, and G. Khaliullin, Phys. Rev. Lett. **105**, 027204 (2010).

[5] S. Calder, V. O. Garlea, D. F. McMorrow, M. D. Lumsden, M. B. Stone, J. C. Lang, J.-W. Kim, J. A. Schlueter, Y. G. Shi, K. Yamaura, Y. S. Sun, Y. Tsujimoto, and A. D. Christianson, Phys. Rev. Lett. **108**, 257209 (2012).

[6] S. Yonezawa, Y. Muraoka, Y. Matsushita, and Z. Hiroi, J. Phys.: Condens. Matter **16**, L9 (2004).

[7] Y. Shi, Y. Guo, S. Yu, M. Arai, A. Sato, A. A. Belik, K. Yamaura, and E. Takayama-Muromachi, J. Am. Chem. Soc. **132**, 8474 (2010).

[8] E. Kan, F. Wu, C. Lee, J. Kang, and M.-H. Whangbo, Inorg. Chem. **50**, 4182 (2011).

[9] J. B. Goodenough, *Magnetism and the Chemical Bond* (Wiley, New York, 1963).

[10] J. Darriet, F. Grasset, and P. D. Battle, Mater. Res. Bull. **32**, 139 (1997).

[11] G. Chen and L. Balents, Phys. Rev. B, **84** 094420 (2011).

[12] A. Wills, Phys. B (Amsterdam) **276**, 680 (2000).

[13] O. V. Kovalev, *Representations of the Crystallographic Space Groups Edition 2* (Gordon and Breach, Switzerland, 1993).

[14] E. E. Rodriguez, F. Poineau, A. Llobet, B. J. Kennedy, M. Avdeev, G. J. Thorogood, M. L. Carter, R. Seshadri, D. J. Singh, and A. K. Cheetham, Phys. Rev. Lett. **106**, 067201 (2011).

[15] J. Mravlje, M. Aichhorn, and A. Georges, Phys. Rev. Lett. **108**, 197202 (2012).

[16] X. Liu, T. Berlijn, W.-G. Yin, W. Ku, A. Tsvelik, Y.-J. Kim, H. Gretarsson, Y. Singh, P. Gegenwart, and J. P. Hill, Phys. Rev. B **83**, 220403 (2011).

[17] D. F. McMorrow, S. E. Nagler, K. A. McEwen, and S. D. Brown, J. Phys.: Condens. Matter **15**, L59 (2003).